Online Appendix: Time-Varying Volatility and the Housing Market

C. Richard Higgins* and Ayse Sapci †

February 10, 2023

*Department of Economics, Colgate University, Hamilton, NY 13346. email: rhiggins@colgate.edu

†Corresponding author. Department of Economics and Finance, Utah State University, 3565 Old Main Hill, Logan, UT 84322. email: ayse.sapci@usu.edu

1 Borrowing Constraints

From entrepreneurs first order conditions we have

$$\frac{1}{\tilde{c}_t} = E_t \left(\gamma \left(\frac{1}{\pi_{t+1} \tilde{c}_{t+1}} \frac{z_t}{z_{t+1}} \right) + \tilde{\lambda}_{b,t} \right) R_t.$$

Therefore, in the steady state

$$\frac{\bar{\pi}}{R} = \frac{\gamma}{g_z} + \lambda_b c \bar{\pi} \tag{1*}$$

holds. From unconstrained households's first order conditions with respect to borrowing we get the following.

$$\tilde{\lambda}_{u,t} - E \beta_u \tilde{\lambda}_{u,t+1} \frac{z_t}{z_{t+1}} \frac{R_t}{\pi_{t+1}} = 0$$

which translates into the following equation in the steady state

$$\frac{\bar{\pi}}{R} = \frac{\beta_u}{g_z}. \tag{2*}$$

Combining Equations 1* and 2* yields

$$\frac{\beta_u}{g_z} = \frac{\gamma}{g_z} + \lambda_b c \bar{\pi}.$$

Given a positive inflation and positive growth (or a negative growth with deflation), for the borrowing constraint to bind ($\lambda_b > 0$), the necessary and sufficient condition is

$$\beta_u > \gamma.$$

Next, from constrained borrowers first order condition with respect to borrowing we have

$$\tilde{\mu}_t - E \beta_c \tilde{\mu}_{t+1} \frac{z_t}{z_{t+1}} \frac{R_t}{\pi_{t+1}} - \tilde{\lambda}_{c,t} R_t = 0,$$

where μ is the budget constraint Lagrangian multiplier and $\lambda_{c,t}$ is the borrowing constraint Lagrangian multiplier.

In the steady state:

$$\mu\left(1-\frac{\beta_c}{g_z}\frac{R}{\bar{\pi}}\right)=\lambda_c R$$

Given the Walrasian budget constraint, positive growth and inflation, for the borrowing constraint of constrained households to bind we need $1>\frac{\beta_c}{g_z}\frac{R}{\bar{\pi}}$ to hold. In other words, $\beta_u>\beta_c$ must be satisfied.

2 Stationary Equilibrium

All the variables are transformed by dividing the corresponding variable to z_t. where $z_t = A_t^{\frac{1}{1-\mu}} x_t^{\frac{\mu}{1-\mu}}$ For example, $\tilde{Y}_t \equiv \frac{Y_t}{z_t}$, $\tilde{c}_t \equiv \frac{c_t}{z_t}, \tilde{b}_t \equiv \frac{b_t}{z_t}$, $\tilde{w}_t \equiv \frac{w_t}{z_t}, \tilde{q}_t \equiv \frac{q_t}{z_t}$, $M_{u,t} \equiv \frac{M_{u,t}}{z_t}$, etc. Investment and capital stock follow $\tilde{I}_t \equiv \frac{I_t}{\chi_t z_t}$, $\tilde{K}_t \equiv \frac{K_t}{\chi_t z_t}$

$$g_{z,t}=\frac{z_t}{z_{t-1}}\rightarrow g_z=\frac{\bar{a}+\mu\bar{\chi}}{1-\mu} \text{ and } g_{x,t}=\frac{\chi_t}{\chi_{t-1}}\rightarrow g_\chi=\bar{\chi}$$

where g_z denotes the steady state value of $g_{z,t}$ and $g_k \equiv g_z g_\chi$ is the steady state rate of capital stock growth. On the balanced growth path, investment grows at the same rate as capital, therefore we have $g_I = g_k$. Additionally, we have $\tilde{\lambda}_{u,t} \equiv \lambda_{u,t} z_t, \tilde{\lambda}_{c,t} \equiv \lambda_{c,t} z_t, \tilde{\mu}_t \equiv \mu_t z_t, \tilde{\lambda}_{b,t} \equiv \lambda_{b,t} z_t$, and $\tilde{u}_t \equiv u_t \chi_t$ and $\tilde{\lambda}_{k,t} \equiv \lambda_{k,t} \chi_t z_t$

Using the transformations indicated above, the full model becomes:

$$\tilde{Y}_t=\left(\frac{A_t\chi_t}{A_{t-1}\chi_{t-1}}\right)^{-\frac{\mu}{1-\mu}}\tilde{K}_{t-1}^{\mu}h_{t-1}^{\nu}L_{u,t}^{\alpha(1-\mu-\nu)}L_{c,t}^{(1-\alpha)(1-\mu-\nu)} \tag{1*}$$

$$\frac{\tilde{Y}_t}{X_t}+\tilde{b}_t=\tilde{c}_t+\tilde{q}_t\left(h_t-h_{t-1}\right)+\frac{R_{t-1}}{\pi_t}\tilde{b}_{t-1}\frac{z_{t-1}}{z_t}+\tilde{w}_{u,t}L_{u,t}+\tilde{w}_{c,t}L_{c,t}+\tilde{I}_t\frac{\psi_H\tilde{q}_t}{2}\left(\frac{h_t-h_{t-1}}{h_{t-1}}\right)^2 h_{t-1} \tag{2*}$$

$$R_t\tilde{b}_t = m_t E_t\left[\tilde{q}_{t+1}\frac{z_{t+1}}{z_t}h_t + \tilde{u}_{t+1}\tilde{K}_t\frac{x_t}{x_{t+1}}\right]\pi_{t+1} \tag{3*}$$

$$\left(1 - \frac{\psi_K}{2}\left(\frac{\tilde{I}_t}{\tilde{I}_{t-1}}\frac{\chi_t z_t}{\chi_{t-1}z_{t-1}} - g_I\right)^2\right)\tilde{I}_t = \tilde{K}_t - (1-\delta)\tilde{K}_{t-1}\frac{\chi_{t-1}z_{t-1}}{\chi_t z_t} \tag{4*}$$

$$\frac{1}{\tilde{c}_t - \zeta\tilde{c}_{t-1}\frac{z_{t-1}}{z_t}} - E_t\frac{\zeta\gamma}{\tilde{c}_{t+1}\frac{z_{t+1}}{z_t} - \zeta\tilde{c}_t} = \tilde{\lambda}_t \tag{5*}$$

$$\tilde{\lambda}_t = E_t\left(\gamma\left(\frac{\tilde{\lambda}_{t+1}}{\pi_{t+1}}\frac{z_t}{z_{t+1}}\right) + \tilde{\lambda}_{b,t}\right)R_t \tag{6*}$$

$$\begin{aligned}\tilde{\lambda}_t = \tilde{\lambda}_{k,t}\Bigg(1 - \frac{\psi_K}{2}\left(\frac{\tilde{I}_t}{\tilde{I}_{t-1}}\frac{\chi_t z_t}{\chi_{t-1}z_{t-1}} - g_I\right)^2 - \psi_K\left(\frac{\tilde{I}_t}{\tilde{I}_{t-1}}\frac{\chi_t z_t}{\chi_{t-1}z_{t-1}} - g_I\right)\frac{\tilde{I}_t}{\tilde{I}_{t-1}}\frac{\chi_t z_t}{\chi_{t-1}z_{t-1}}\Bigg) \\ + E_t\gamma\tilde{\lambda}_{k,t+1}\frac{z_t\chi_t}{z_{t+1}\chi_{t+1}}\psi_K\left(\frac{\tilde{I}_{t+1}}{\tilde{I}_t}\frac{\chi_{t+1}z_{t+1}}{\chi_t z_t} - g_I\right)\left(\frac{\tilde{I}_{t+1}}{\tilde{I}_t}\frac{\chi_{t+1}z_{t+1}}{\chi_t z_t}\right)^2\end{aligned} \tag{7*}$$

$$E_t\left(\tilde{\lambda}_{t+1}\gamma\frac{\mu\tilde{Y}_{t+1}}{X_{t+1}\tilde{K}_t} + \tilde{\lambda}_{b,t}m_t\tilde{u}_{t+1}\frac{z_{t+1}}{z_t}\frac{\chi_t}{\chi_{t+1}}\pi_{t+1} - \frac{z_{t+1}}{z_t}\tilde{\lambda}_{k,t} + \tilde{\lambda}_{k,t+1}\frac{\chi_t}{\chi_{t+1}}\gamma(1-\delta)\right) = 0 \tag{8*}$$

$$\begin{aligned}\tilde{q}_t\tilde{\lambda}_t\left(1 + \psi_H\left(\frac{h_t - h_{t-1}}{h_{t-1}}\right)\right) = E_t\left(\gamma\tilde{\lambda}_{t+1}\left(\frac{\nu\tilde{Y}_{t+1}}{X_{t+1}h_t} + \tilde{q}_{t+1} + \frac{1}{2}\psi_H\tilde{q}_{t+1}\left(\frac{h_{t+1}^2 - h_t^2}{h_t^2}\right)\right)\right) \\ + E_t\left(\tilde{\lambda}_{b,t}m_t\tilde{q}_{t+1}\frac{z_{t+1}}{z_t}\pi_{t+1}\right)\end{aligned} \tag{9*}$$

$$\frac{\alpha(1-\mu-\nu)\tilde{Y}_t}{X_t L_{u,t}} = \tilde{w}_{u,t} \tag{10*}$$

$$\frac{(1-\alpha)(1-\mu-\nu)\tilde{Y}_t}{X_t L_{c,t}} = \tilde{w}_{c,t} \tag{11*}$$

$$\begin{aligned}\tilde{c}_{u,t}+\tilde{q}_t\left(h_{u,t}-h_{u,t-1}\right)+\frac{R_{t-1}}{\pi_t}\tilde{b}_{u,t-1}\frac{z_{t-1}}{z_t}+\frac{\psi_H\tilde{q}_t}{2}\left(\frac{h_{u,t}-h_{u,t-1}}{h_{u,t-1}}\right)^2 h_{u,t-1}\\ =\tilde{b}_{u,t}+\tilde{w}_{u,t}L_{u,t}+\tilde{F}_t-\left(\frac{\tilde{M}_{u,t}-\tilde{M}_{u,t-1}\frac{z_{t-1}}{z_t}}{P_{u,t}}\right)+\tilde{T}_{u,t}\end{aligned} \tag{12*}$$

$$\frac{\varrho_t}{\tilde{c}_{u,t}-\zeta\tilde{c}_{u,t-1}\frac{z_{t-1}}{z_t}}-E_t\frac{\zeta\beta_u\varrho_{t+1}}{\tilde{c}_{u,t+1}\frac{z_{t+1}}{z_t}-\zeta\tilde{c}_{u,t}}=\tilde{\lambda}_{u,t} \tag{13*}$$

$$\tilde{\lambda}_{u,t}-E_t\beta_u\tilde{\lambda}_{u,t+1}\frac{z_t}{z_{t+1}}\frac{R_t}{\pi_{t+1}}=0 \tag{14*}$$

$$\tilde{\lambda}_{u,t}\tilde{q}_t\left(1+\psi_{H,u}\frac{h_{u,t}-h_{u,t-1}}{h_{u,t-1}}\right)=\varrho_t\frac{j_u}{h_{u,t}}+E_t\beta_u\tilde{\lambda}_{u,t+1}\tilde{q}_{t+1}\left(\frac{\psi_{H,u}^2}{\left(\frac{h_{u,t+1}^2-h_{u,t}^2}{h_{u,t}^2}\right)+1}\right) \tag{15*}$$

$$\tilde{\lambda}_{u,t}\tilde{w}_{u,t}=\varrho_t\varphi_t\left(L_{u,t}\right)^{\eta\prime-1} \tag{16*}$$

$$\begin{aligned}\tilde{c}_{c,t}+\tilde{q}_t\left(h_{c,t}-h_{c,t-1}\right)+\frac{R_{t-1}}{\pi_t}\tilde{b}_{c,t-1}\frac{z_{t-1}}{z_t}+\frac{\psi_H\tilde{q}_t}{2}\left(\frac{h_t-h_{t-1}}{h_{t-1}}\right)^2 h_{t-1}\\ =\tilde{b}_{c,t}+\tilde{w}_{c,t}L_{c,t}-\left(\frac{\tilde{M}_{c,t}-\tilde{M}_{c,t-1}\frac{z_{t-1}}{z_t}}{P_t}\right)+\tilde{T}_{c,t}\end{aligned} \tag{17*}$$

$$R_t\tilde{b}_{c,t}\leq E_t\left\{m_{c,t}\tilde{q}_{t+1}\frac{z_{t+1}}{z_t}h_{c,t}\pi_{t+1}\right\} \tag{18*}$$

$$\frac{\varrho_t}{\tilde{c}_{c,t}-\zeta\tilde{c}_{c,t-1}\frac{z_{t-1}}{z_t}}-E_t\frac{\zeta\beta_c\varrho_{t+1}}{\tilde{c}_{c,t+1}\frac{z_{t+1}}{z_t}-\zeta\tilde{c}_{c,t}}=\tilde{\mu}_t \tag{19*}$$

$$\tilde{\mu}_t-E_t\beta_c\tilde{\mu}_{t+1}\frac{z_t}{z_{t+1}}\frac{R_t}{\pi_{t+1}}-\tilde{\lambda}_{c,t}R_t=0 \tag{20*}$$

$$\tilde{\mu}_t \tilde{q}_t \left(1 + \psi_{H,c} \left(\frac{h_{c,t} - h_{c,t-1}}{h_{c,t-1}}\right)\right)$$
$$= \varrho_t \frac{j_c}{h_{c,t}} + E_t \left\{\beta_c \tilde{q}_{t+1} \tilde{\mu}_{t+1} \left(\frac{\psi_{H,c}}{2} \left(\frac{h_{c,t+1}^2 - h_{c,t}^2}{h_{c,t}^2}\right) + 1\right) + \tilde{\lambda}_{c,t} m_{c,t} \tilde{q}_{t+1} \frac{z_{t+1}}{z_t} \pi_{t+1}\right\} \quad (21^*)$$

$$\tilde{w}_{c,t} \tilde{\mu}_t = \varrho_t \varphi_t \left(L_{c,t}\right)^{\eta_c - 1} \quad (22^*)$$

$$\tilde{F}_t = \frac{\left(X_t - 1\right) \tilde{Y}_t}{X_t} \quad (23^*)$$

$$1 = h_t + h_{u,t} + h_{c,t} \quad (24^*)$$

$$\tilde{Y}_t = \tilde{c}_t + \tilde{c}_{u,t} + \tilde{c}_{c,t} + \tilde{I}_t + \frac{\psi_H \tilde{q}_t}{2} \left(\frac{h_t - h_{t-1}}{h_{t-1}}\right)^2 h_{t-1} \quad (25^*)$$

$$0 = \tilde{b}_t + \tilde{b}_{u,t} + \tilde{b}_{c,t} \quad (26^*)$$

$$\tilde{u}_t = \frac{\tilde{\lambda}_{k,t}}{\tilde{\lambda}_t} \quad (27^*)$$

$$\tilde{\lambda}_t = \frac{1}{\tilde{c}_t} \quad (28^*)$$

$$g_t^1 = \tilde{\lambda}_{u,t} \left(\pi_t^*\right)^{(1-\varepsilon)} \tilde{Y}_t + \beta_u \theta E_t \left(\frac{\pi_t^*}{\pi_{t+1}^* \pi_{t+1}}\right)^{1-\varepsilon} g_{t+1}^1 \quad (29^*)$$

$$g_t^2 = \tilde{\lambda}_{u,t} \left(\pi_t^*\right)^{-\varepsilon} \frac{\tilde{Y}_t}{X_t} + \beta_u \theta E_t \left(\frac{\pi_t^*}{\pi_{t+1}^* \pi_{t+1}}\right)^{-\varepsilon} g_{t+1}^2 \quad (30^*)$$

3 Steady State

$$\pi = \bar{\pi} \tag{1*}$$

$$R = \frac{1}{\beta_u}\bar{\pi} g_z \tag{2*}$$

$$X = \frac{\varepsilon}{\varepsilon - 1} \tag{3*}$$

$$\frac{\tilde{F}}{\tilde{Y}} = \left(1 - \frac{1}{X}\right) \tag{4*}$$

$$\frac{\tilde{K}}{\tilde{Y}} = \gamma \frac{\mu}{X} \frac{1}{g_z - (\beta' - \gamma)\, m \frac{1}{g_\chi} - \frac{1}{g_\chi}\gamma(1-\delta)} \equiv \zeta_1 \tag{5*}$$

$$\frac{\tilde{I}}{\tilde{Y}} = \frac{\tilde{K}}{\tilde{Y}} \left(1 - (1-\delta)\frac{1}{g_z g_\chi}\right) \tag{6*}$$

$$\frac{\tilde{c} + \tilde{c_u} + \tilde{c_c}}{\tilde{Y}} = 1 - \frac{\tilde{I}}{\tilde{Y}} \tag{7*}$$

$$\frac{\tilde{q}h}{\tilde{Y}} = \frac{1}{X} \frac{\gamma\nu}{1 - (\beta_u - \gamma)\, m - \gamma} \equiv \zeta_2 \tag{8*}$$

$$\frac{\frac{\tilde{q}h_u}{\tilde{Y}}}{\frac{\tilde{c_u}}{\tilde{Y}}} = \frac{j_u\,(g_z - \zeta)}{(g_z - \zeta\beta_u)\,(1 - \beta_u)} \equiv \zeta_3 \tag{9*}$$

$$\frac{\frac{\tilde{q}h_c}{\tilde{Y}}}{\frac{\tilde{c_c}}{\tilde{Y}}} = \frac{j_c\,(g_z - \zeta)}{(g_z - \zeta\beta_c)\,(1 - \beta_c - m_c\,(\beta_u - \beta_c))} \equiv \zeta_4 \tag{10*}$$

$$\frac{\tilde{b}}{\tilde{Y}} = \beta_u m \left(\frac{\tilde{q}h}{\tilde{Y}} + \frac{\tilde{K}}{\tilde{Y}} \frac{1}{g_z g_x}\right) \tag{11*}$$

$$\frac{\tilde{w}\tilde{L_u}+F}{\tilde{Y}}=\frac{\alpha(1-\mu-\nu)+X-1}{X}\equiv s_u \tag{12*}$$

$$\frac{\tilde{w_c}\tilde{L_c}}{\tilde{Y}}=\frac{(1-\alpha)(1-\mu-\nu)}{X}\equiv s_c \tag{13*}$$

$$\frac{\tilde{c}}{\tilde{Y}}=\frac{\mu+\nu}{X}-(1-\beta_u)m\zeta_2-\left((m(1-\beta_u)-(1-\delta))\frac{1}{g_z g_\chi}+1\right)\zeta_1\equiv\zeta_5 \tag{14*}$$

$$\frac{\frac{\tilde{b_c}}{\tilde{Y}}}{\frac{\tilde{c_c}}{\tilde{Y}}}=\beta_u m_c\zeta_4 \tag{15*}$$

$$\frac{\tilde{c_c}}{\tilde{Y}}=\frac{s_c}{1+(1-\beta_u)m_c\zeta_4}\equiv\zeta_6 \tag{16*}$$

$$\frac{\tilde{c_u}}{\tilde{Y}}=s_u+(1-\beta_u)\left(m\left(\zeta_2+\zeta_1\frac{1}{g_z g_\chi}\right)+m_c\zeta_4\zeta_6\right)\equiv\zeta_7 \tag{17*}$$

$$h=\frac{\zeta_2}{\zeta_3\zeta_7+\zeta_4\zeta_6+\zeta_2} \tag{18*}$$

$$h_u=\frac{\zeta_3\zeta_7}{\zeta_3\zeta_7+\zeta_4\zeta_6+\zeta_2} \tag{19*}$$

$$h_c=\frac{\zeta_4\zeta_6}{\zeta_3\zeta_7+\zeta_4\zeta_6+\zeta_2} \tag{20*}$$

$$L_u=\left(\frac{\alpha(1-\mu-\nu)(g_z-\zeta\beta_u)}{\tilde{X}(g_z-\zeta)\frac{\tilde{c}_u}{\tilde{Y}}}\right)^{\frac{1}{\eta_u}} \tag{21*}$$

$$L_c=\left(\frac{(1-\alpha)(1-\mu-\nu)}{\tilde{X}}\frac{g_z-\zeta\beta_c}{(g_z-\zeta)\frac{\tilde{c_c}}{\tilde{Y}}}\right)^{\frac{1}{\eta_c}} \tag{22*}$$

$$\tilde{Y} = \left((\bar{a}\bar{\chi})^{-\frac{\mu}{1-\mu}} \left(\frac{\tilde{K}}{\tilde{Y}} \right)^{\mu} h^{\nu} L_u^{\alpha(1-\mu-\nu)} L_c^{(1-\alpha)(1-\mu-\nu)} \right)^{\frac{1}{1-\mu}} \tag{23*}$$

4 Estimation Procedure

The estimation procedure follows Fernández-Villaverde et al. (2015), who show that models with stochastic volatility can be estimated without measurement error. To do this, we first define the structural shocks are as

$$\mathcal{Z}_t = (\log \widetilde{\chi}_t, \log j_t, \log m_t, \log \widetilde{A}_t, \log \omega, t, \log \varrho_t, \log \varphi_t)'.$$

The structural shocks are assumed to follow the process below.

$$\mathcal{Z}_{it+1} = \rho_i \mathcal{Z}_{it} + \Lambda \sigma_i \sigma_{it+1} \epsilon_{it+1} \tag{1}$$

for all $i \in 1, ..., m$ where σ_{it+1} denotes the stochastic volatility shock and Λ represents the perturbation parameter. The stochastic volatility shocks evolve as

$$\log \sigma_{it+1} = \rho_{\sigma_i} \log \sigma_{it} + \Lambda \left(1 - \rho_{\sigma_i}^2\right)^{\frac{1}{2}} \eta_i u_{it+1}. \tag{2}$$

Next, we put the approximated model into a state space representation. The endogenous state vector evolves as

$$\mathcal{S}_{t+1} = h\left(\mathcal{S}_t, \mathcal{Z}_{t-1}, \Sigma_{t-1}, \mathcal{E}_t, \mathcal{U}_t, \Lambda; \gamma\right) \tag{3}$$

while two policy functions evolve according to the following processes

$$\mathcal{Y}_t = g\left(\mathcal{S}_t, \mathcal{Z}_{t-1}, \Sigma_{t-1}, \mathcal{E}_t, \mathcal{U}_t, \Lambda; \gamma\right) \tag{4}$$

$$\mathcal{Y}_{t+1} = g\left(\mathcal{S}_{t+1}, \mathcal{Z}_t, \Sigma_t, \Lambda\mathcal{E}_{t+1}, \Lambda\mathcal{U}_{t+1}, \Lambda; \gamma\right). \tag{5}$$

The functions h and g map $\mathbb{R}^{n+4m}$ into $\mathbb{R}^n$ and $\mathbb{R}^k$. The vector of volatility shocks is defined as

$$\Sigma_t = (\widehat{\sigma}_{X,t}, \widehat{\sigma}_{J,t}, \widehat{\sigma}_{m,t}, \widehat{\sigma}_{A,t}, \widehat{\sigma}_{\omega,t}, \widehat{\sigma}_{\varrho,t}, \widehat{\sigma}_{\varphi,t})'$$

where $\widehat{\sigma}_{x,t} = \sigma_{x,t}/\sigma_x$. The innovations are divided between an $m \times 1$ vector of innovation to structural shocks, $\mathcal{E}_t$ and an $(m) \times 1$ vector of innovations to volatility shocks, $\mathcal{U}_t$. For this model, the vector of innovations are defined as

$$\mathcal{E}_t = (\varepsilon_{Xt}, \varepsilon_{Jt}, \varepsilon_{mt}, \varepsilon_{At}, \varepsilon_{\omega t}, \varepsilon_{\varrho t}, \varepsilon_{\varphi t})'$$

and

$$\mathcal{U}_t = (u_{Xt}, u_{Jt}, u_{mt}, u_{At}, u_{\omega t}, u_{\varrho t}, u_{\varphi t})'.$$

As in Fernández-Villaverde et al. (2015), equations 1 to 3 are stacked into the following transition equation

$$\mathbb{S}_{t+1} = \tilde{h}(\mathbb{S}_t, \Lambda; \gamma) + \Xi \mathbb{W}_{t+1} \tag{6}$$

where $\mathbb{S}_t = \left(\mathcal{S}_t', \mathcal{Z}_{t-1}', \Sigma_t', \mathcal{E}_{t-1}', \mathcal{U}_{t-1}'\right)'$ and $\tilde{h}$ maps $\mathbb{R}^{n+4m-2p+1}$ into $\mathbb{R}^{n+4m-2p}$. The vector $\mathbb{W}_{t+1} = \left(\mathcal{W}_{1t+1}', \mathcal{W}_{2t+1}'\right)'$ is a $(2m-p) \times 1$ vector of random variables, where $\mathcal{W}_{1t+1}$ and $\mathcal{W}_{2t+1}$ are, respectively, $m \times 1$ and $(m-p) \times 1$ vectors with $N(0, I)$ distributions. The random variables $\mathcal{W}_1$ align with the innovations to the shocks and the random variables $\mathcal{W}_2$ align with the innovations to the stochastic volatility shocks. Ξ is an $(n+4m-2p) \times (2m-p)$ matrix, where the top $n+2m-p$ rows equal to zero and the bottom of the matrix equal to a $(2m-p) \times (2m-p)$ identity matrix. The policy function can also be rewritten as

$$\mathcal{Y}_t = g\left(\mathbb{S}_t, \Lambda; \gamma\right). \tag{7}$$

Equations 6 and 7 are approximated around the steady-state using the perturbation method to find a second-order approximation. The approximate solution then is used to calculate the likelihood of $\mathbb{Y}^T = (\mathbb{Y}_1, ..., \mathbb{Y}_T)$, where $\mathbb{Y}_t$ is the data counterpart to the observable $\mathcal{Y}_t$ in the

model. The likelihood can be written as

$$\prod_{t=1}^{T} p\left(\mathcal{Y}_t = \mathbb{Y}_t | \mathbb{Y}^{t-1}; \gamma\right) \tag{8}$$

where

$$p\left(\mathcal{Y}_t = \mathbb{Y}_t | \mathbb{Y}^{t-1}; \gamma\right) = \int\int\int\int p\left(\mathcal{Y}_t = \mathbb{Y}_t | \mathcal{S}_t, \mathcal{Z}_{t-1}, \Sigma_{t-1}, \mathcal{E}_t; \gamma\right) p\left(\mathcal{S}_t, \mathcal{Z}_{t-1}, \Sigma_{t-1}, \mathcal{E}_t | \mathbb{Y}^{t-1}; \gamma\right) d\mathcal{S}_t d\mathcal{Z}_{t-1} d\Sigma_{t-1} d\mathcal{E}_t \tag{9}$$

for all $t \in \{2, ..., T\}$ and

$$p\left(\mathcal{Y}_1 = \mathbb{Y}_1 | \mathbb{Y}^{t-1}; \gamma\right) = \int\int\int\int p\left(\mathcal{Y}_1 = \mathbb{Y}_1 | \mathcal{S}_1, \mathcal{Z}_0, \Sigma_0, \mathcal{E}_1; \gamma\right) p\left(\mathcal{S}_1, \mathcal{Z}_0, \Sigma_0, \mathcal{E}_1 | \gamma\right) d\mathcal{S}_1 d\mathcal{Z}_0 d\Sigma_0 d\mathcal{E}_1. \tag{10}$$

Since there is not an analytical solution to the likelihood, a particle filter is used in order to evaluate the likelihood.

Fernández-Villaverde et al. (2015) show that the difference between the observed variables and the approximated observation equation can be written as

$$\mathbb{A}_t\left(\mathbb{Y}_t, s_t^i, z_{t-1}^i, \sigma_{t-1}^i, \varepsilon_t^i\right) =$$

$$\mathbb{Y}_t - \mathcal{Y} - \begin{pmatrix} \tilde{\Psi}^1_{Y1} \tilde{\tilde{\mathbb{S}}}_t^i \\ \vdots \\ \tilde{\Psi}^1_{Yk} \tilde{\tilde{\mathbb{S}}}_t^i \end{pmatrix} + \frac{1}{2} \begin{pmatrix} \tilde{\tilde{\mathbb{S}}}_t^{i\prime} \tilde{\Psi}^{2,1}_{\mathcal{Y},1} \tilde{\tilde{\mathbb{S}}}_t^i \\ \vdots \\ \tilde{\tilde{\mathbb{S}}}_t^{i\prime} \tilde{\Psi}^{2,1}_{\mathcal{Y},k} \tilde{\tilde{\mathbb{S}}}_t^i \end{pmatrix} + \frac{1}{2} \begin{pmatrix} \Psi^{\Lambda}_{\mathcal{Y},1} \\ \vdots \\ \Psi^{\Lambda}_{\mathcal{Y},k} \end{pmatrix} + \begin{pmatrix} \varepsilon_t^{i\prime} \tilde{\Psi}^{2,2}_{\mathcal{Y},1} \\ \vdots \\ \varepsilon_t^{i\prime} \tilde{\Psi}^{2,2}_{\mathcal{Y},k} \end{pmatrix} \sigma_{t-1}^i$$

where $\tilde{\mathbb{S}}_t^i = \left(s_t^{i\prime}, z_{t-1}^{i\prime}, \sigma_{t-1}^{i\prime}, \varepsilon_t^{i\prime}\right)'$ represents the simulated states without the stochastic volatility components and $\tilde{\tilde{\mathbb{S}}}_t^i$ represents these states in deviation from the mean form. Also, $\tilde{\Psi}^1_{Yj}$ represents the first-order components of the approximation to the observation equation that relates to $\tilde{\tilde{\mathbb{S}}}_t^i$, while $\tilde{\Psi}^{2,1}_{\mathcal{Y},j}$ represents the second order components relating to $\tilde{\tilde{\mathbb{S}}}_t^i$, $\Psi^{\Lambda}_{\mathcal{Y},j}$ represents the

linear terms of the approximation, and $\tilde{\Psi}^{2,2}_{\mathcal{Y},j}$ represents the second order components related to the innovations to the shocks and stochastic volatility shocks for $j = 1, ..., k$. It is important to also define

$$\mathbb{B}\left(\varepsilon_t\right) = \begin{pmatrix} \varepsilon_t^{i'} \tilde{\Psi}^{2,2}_{\mathcal{Y},1} \\ \vdots \\ \varepsilon_t^{i'} \tilde{\Psi}^{2,2}_{\mathcal{Y},k} \end{pmatrix}. \tag{11}$$

These equations are used to calculate the measurement density as

$$p\left(\mathcal{Y}_t = \mathbb{Y}_t | s_t^i, z_{t-1}^i, \sigma_{t-1}^i; \gamma\right) =$$

$$\left|\det\left(\mathbb{B}^{-1}\left(\varepsilon_t^{i'}; \gamma\right)\right)\right| p\left(\left(\mathcal{U}_t\right) = \mathbb{B}^{-1}\left(\varepsilon_t^{i'}; \gamma\right) \mathbb{A}_t\left(s_t^i, z_{t-1}^i, \sigma_{t-1}^i, \varepsilon_t^{i'}; \gamma\right)\right). \tag{12}$$

This can be evaluated since the distribution of $\mathcal{U}_t$ is known. The measurement density can be applied to the particle filter in order to approximate the likelihood.

4.1 Particle Filter

The particle filter follows Fernández-Villaverde et al. (2015), but adds a mutation resample-move step and adaption for some periods. Since the model does not feature measurement error, **?** show that sample impoverishment, where there is little diversity in the particle swarm after resampling, is a concern. A resample-move step, which can be seen in steps 3-5 of the code below, is used to reduce the amount of impoverishment. Another concern with the particle filter is not having enough draws from the tails of the distribution of random shocks during extreme events, like the global financial crisis and, to a lesser extend, the time following the dot-com bubble bursting. Adaption is used during the time periods 1999:Q4-2001:Q1 and 2005:Q1-2011:Q4. The details of the particle filter are described in the following paragraphs.

- **Initialization** Set $t \rightsquigarrow 1$. Sample N values $\{s_t^i, z_{t-1}^i, \sigma_{t-1}^i, \varepsilon_t^i\}_{i=1}^N$ from $p\left(\mathcal{S}_t, \mathcal{Z}_{t-1}, \Sigma_{t-1}, \mathcal{E}_t; \gamma\right)$.

- **Step 1** Compute

$$p\left(\mathcal{Y}_t = \mathbb{Y}_t | s_t^i, z_{t-1}^i, \sigma_{t-1}^i, \varepsilon_t^i; \gamma\right) \simeq$$

$$\frac{1}{N}\sum_{i=1}^{N}\left|\det\left(\mathbb{B}^{-1}\left(\varepsilon_t^{i'};\gamma\right)\right)\right| p\left(\left(\mathcal{U}_t\right) = \mathbb{B}^{-1}\left(\varepsilon_t^{i'};\gamma\right)\mathbb{A}_t\left(s_t^i, z_{t-1}^i, \sigma_{t-1}^i, \varepsilon_t^{i'};\gamma\right)\right)$$

and define importance weights for each draw as

$$q_t^i = \frac{\left|\det\left(\mathbb{B}^{-1}\left(\varepsilon_t^{i'};\gamma\right)\right)\right| p\left(\left(\mathcal{U}_t\right) = \mathbb{B}^{-1}\left(\varepsilon_t^{i'};\gamma\right)\mathbb{A}_t\left(s_t^i, z_{t-1}^i, \sigma_{t-1}^i, \varepsilon_t^{i'};\gamma\right)\right)}{\sum_{i=1}^{N}\left|\det\left(\mathbb{B}^{-1}\left(\varepsilon_t^{i'};\gamma\right)\right)\right| p\left(\left(\mathcal{U}_t\right) = \mathbb{B}^{-1}\left(\varepsilon_t^{i'};\gamma\right)\mathbb{A}_t\left(s_t^i, z_{t-1}^i, \sigma_{t-1}^i, \varepsilon_t^{i'};\gamma\right)\right)}.$$

- **Step 2** Sample N times with replacement from $\{s_{t|t-1}^i, z_{t-1|t-1}^i, \sigma_{t-1|t-1}^i, \varepsilon_{t|t-1}^i\}_{i=1}^N$ using weights given by $\{q_t^i\}_{i=1}^N$. Define the draws as $\{s_{t|t}^i, z_{t-1|t}^i, \sigma_{t-1|t}^i, \hat{\varepsilon}_{t|t}^i\}_{i=1}^N$.

- **Step 3** Draw N vectors, ϵ_t^i, from the distribution $N\left(0, 0.15I\right)$ and calculate $\tilde{\varepsilon}_{t|t}^i = \hat{\varepsilon}_{t|t}^i + \epsilon_t^i$.

- **Step 4** Compute

$$p\left(\mathcal{Y}_t | s_t^i, z_{t-1}^i, \sigma_{t-1}^i, \tilde{\varepsilon}_t^i\ ; \gamma\right) =$$

$$\left|\det\left(\mathbb{B}^{-1}\left(\tilde{\varepsilon}_t^{i'};\gamma\right)\right)\right| p\left(\left(\mathcal{U}_t\right) = \mathbb{B}^{-1}\left(\tilde{\varepsilon}_t^{i'};\gamma\right)\mathbb{A}_t\left(s_t^i, z_{t-1}^i, \sigma_{t-1}^i, \tilde{\varepsilon}_t^{i'};\gamma\right)\right)$$

- **Step 5** For $i = 1 : N$, set $\{s_{t|t}^i, z_{t-1|t}^i, \sigma_{t-1|t}^i, \varepsilon_{t|t}^i\}$ to $\{s_{t|t}^i, z_{t-1|t}^i, \sigma_{t-1|t}^i, \tilde{\varepsilon}_{t|t}^i\}$ with probability

$$\alpha = \min\{1, \frac{p\left(\mathcal{Y}_t | s_t^i, z_{t-1}^i, \sigma_{t-1}^i, \tilde{\varepsilon}_t^i\ ; \gamma\right) p\left(\tilde{\varepsilon}_t^i\right)}{p\left(\mathcal{Y}_t | s_t^i, z_{t-1}^i, \sigma_{t-1}^i, \hat{\varepsilon}_t^i\ ; \gamma\right) p\left(\hat{\varepsilon}_t^i\right)}\}$$

where $p\left(\tilde{\varepsilon}_t^i\right)$ and $p\left(\hat{\varepsilon}_t^i\right)$ are calculated based on a $N\left(0, I\right)$ distribution. Otherwise, set $\{s_{t|t}^i, z_{t-1|t}^i, \sigma_{t-1|t}^i, \varepsilon_{t|t}^i\}$ to $\{s_{t|t}^i, z_{t-1|t}^i, \sigma_{t-1|t}^i, \hat{\varepsilon}_{t|t}^i\}$.

- **Step 6** Simulate $\{s_{t+1}^i, z_t^i, \sigma_t^i, \varepsilon_{t+1}^i\}_{i=1}^N$ using $\{s_{t|t}^i, z_{t-1|t}^i, \sigma_{t-1|t}^i, \varepsilon_{t|t}^i\}_{i=1}^N$ by making N draws of ε_t from the distribution $N\left(0, I\right)$.

- **Step 7** If $t < T$, set $t \rightsquigarrow t + 1$ and go to step 1. Otherwise stop.

The filter is implemented using 15,000 particles. As discussed by Fernández-Villaverde and Rubio-Ramírez (2007), it is important to use the same random numbers used for innovations

as new draws in the Metropolis Hastings algorithm. In order to avoid biasing the results based on the random numbers drawn, the random numbers used for the resample step are different across draws. Since this procedure creates some noise in the calculation of the likelihood, it is calculated for both the current draw and the candidate draw of parameters each step of the algorithm. This method avoids the possibility of obtaining an unusually high calculated likelihood, and therefore an unusually high posterior, which would result in rejecting many candidate draws from parameters that may have similar posteriors.

Adaption is only used during the time periods 1999:Q4-2001:Q1 and 2005:Q1-2011:Q4.[1] The particle filter would frequently degenerate without adaption during these periods, since there were not enough draws from the tails of the distribution. To avoid degeneration, we adapt the particle filter during these time periods as in Gust et al. (2017). The random draws of the innovations to the traditional shocks, $\mathcal{W}_{1,t}$, are drawn from the distribution $N(0, \Sigma)$, where $\Sigma = 1.5I$, during these time periods instead of $N(0, I)$ as in all other time periods.[2] As shown in Gust et al. (2017), this must be accounted for by re-weighting the likelihood and importance weights by the factor

$$\kappa = \frac{\exp\left(-\frac{1}{2}\varepsilon_t^{i'}\varepsilon_t^i\right)}{|\Sigma|^{-\frac{1}{2}}\exp\left(\varepsilon_t^i\Sigma^{-1}\varepsilon_t^{i'}\right)}. \tag{13}$$

4.2 Implementation details

The particle filter described above is very time consuming, especially for a model of this size. To save time, the derivatives of the model needed to measure the approximation are calculated in MATLAB using the symbolic toolbox which are then saved as functions. The estimation is run within MATLAB using C code and LAPACK to save time and be more efficient with memory. The algorithm used in this paper does not use parallel code in the particle filter so that prefetching can be used in the Metropolis Hastings algorithm. This strategy also allows us to estimate more specifications of the model at one time. Performing 25,000 draws of the Metropolis Hastings algorithm takes approximately 293 hours.

[1] We choose not to use a methodology that adapts for every time period, like Plante et al. (2017), because computation of the likelihood is already very taxing and time consuming.

[2] The value of $\Sigma = 1.5I$ was selected after extensive testing.

5 Prior and Posterior Distribution Comparison

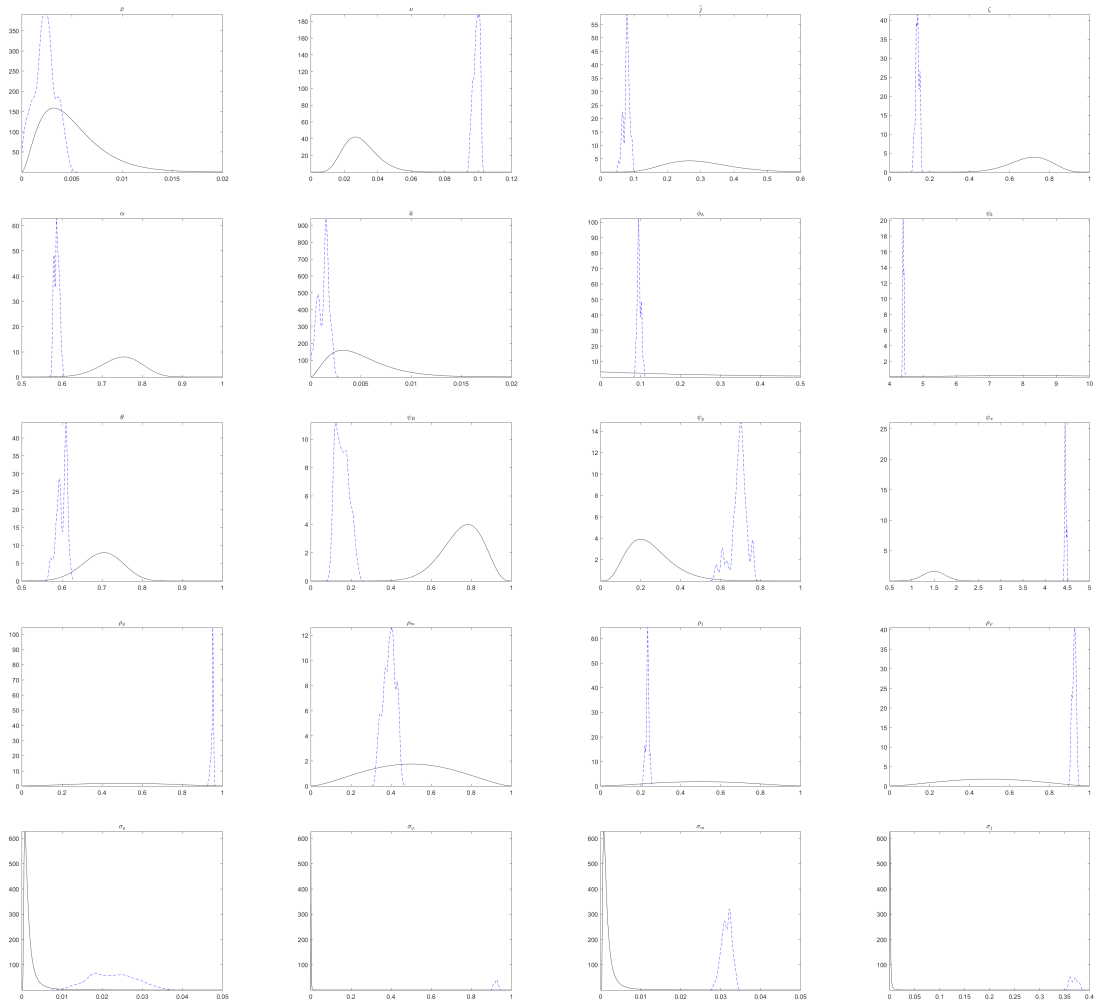

Figure 1: Prior Distributions (Solid Lines) vs. Kernel Density of the Posterior Draws (Blue, Dashed Lines)

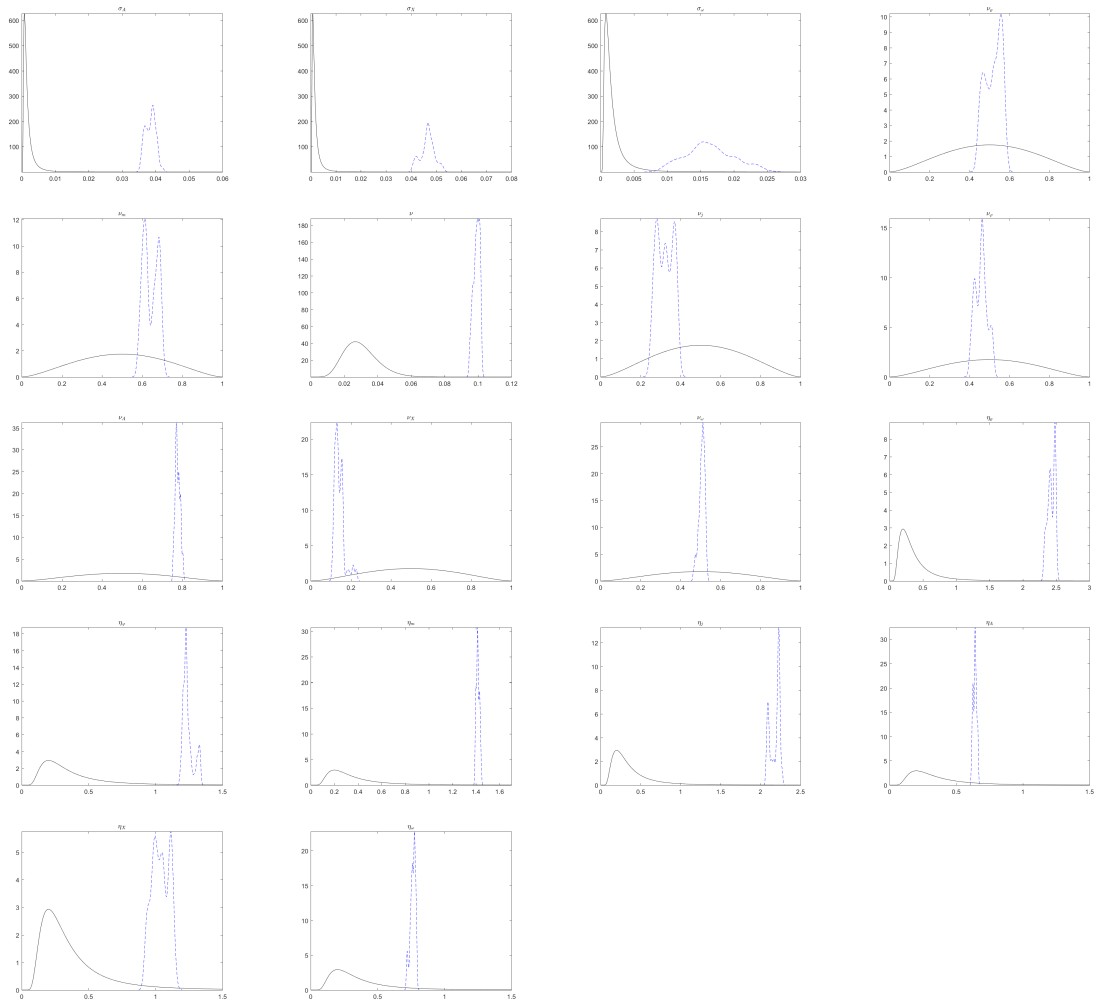

Figure 2: Prior Distributions (Solid Lines) vs. Kernel Density of the Posterior Draws (Blue, Dashed Lines)

6 Running Mean Plots

The figures below show plots of the running means from the Metropolis Hastings algorithm for each parameter. These figures show that the estimates have converged.

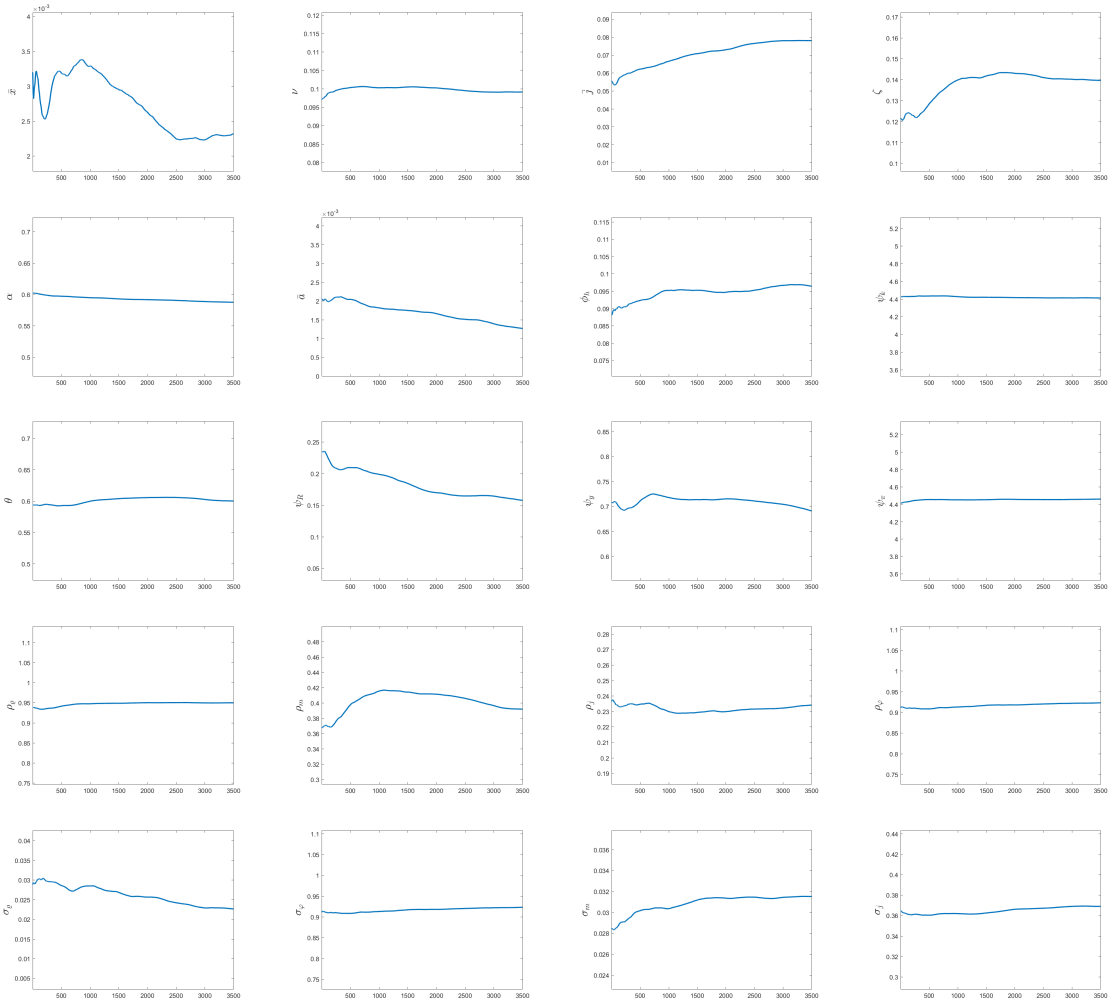

Figure 3: Running Mean Plots

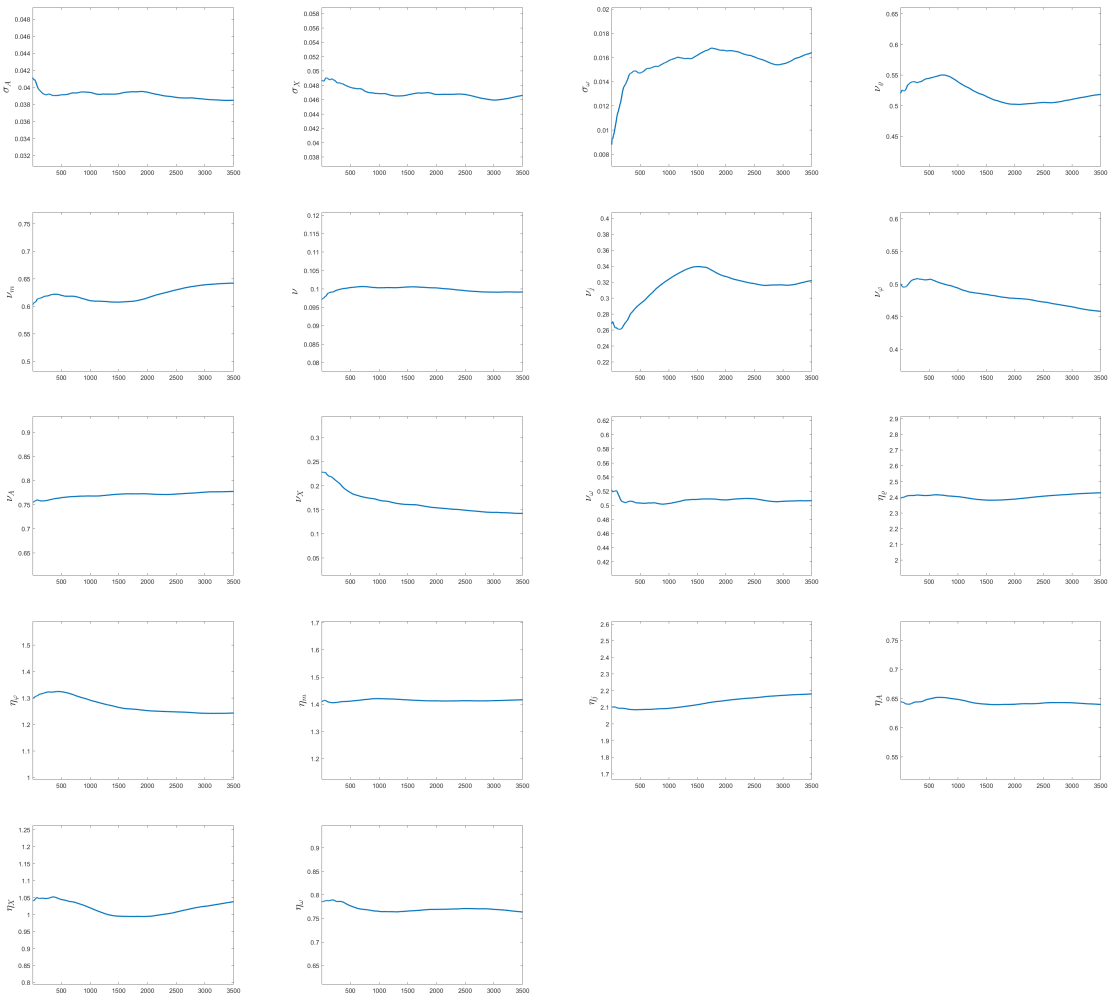

Figure 4: Running Mean Plots

7 Underlying States: Confidence Bands

Figure 5: Underlying States: Level Shocks

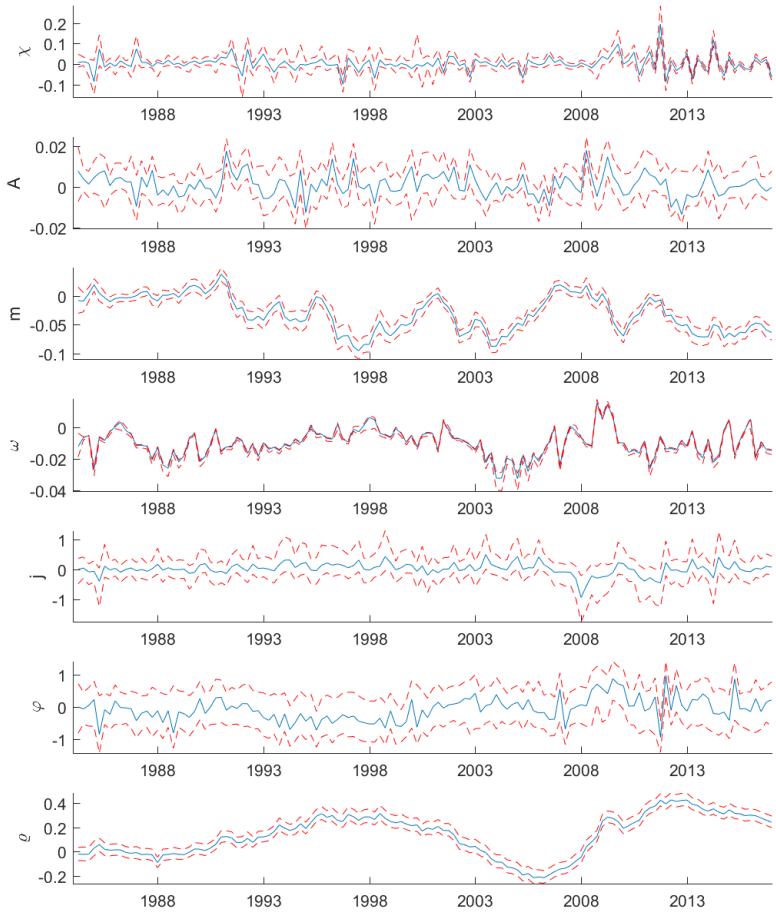

Note: Smoothed underlying states of the traditional shocks in log deviation from the mean form. These are calculated at the posterior mode. The solid, blue line represents the median, while the red, dashed line represent the 20^{th} and 80^{th} percentiles.

Figure 6: Underlying States: Stochastic Volatility

Note: Smoothed underlying states of the stochastic volatility shocks in log deviation from the mean form. The solid, blue line represents the median, while the red, dashed line represent the 20^{th} and 80^{th} percentiles.

8 Robustness: Alternative Calibrations

In the model, we have a total of 46 parameters and we only calibrate 9 of them. Among these nine parameters, capital depreciation, labor share of production, average loan to value ratio, and the steady state gross inflation rate are based on U.S. data and are commonly used in the literature as described in Section 4 of the main paper. The discount factors, the weight of labor utility, and the monopoly power, are more model specific that we base our choice of values on the previous research. This section explores the importance of fixing these parameters.

To do this, we study three alternative calibrations. The first calibration sets the discount factors of the entrepreneurs and unconstrained households to lower values than used in the benchmark case, with $\beta_u = 0.985$ and $\gamma = 0.975$ instead of 0.99 and 0.98, respectively. The second calibration lowers the weight of labor in the utility function and the level of monopoly power, setting $\eta_c = \eta_u = 2$ instead of 2.17 and $\epsilon = 11$ instead of 21. The third calibration lowers the discount factor of constrained households, setting $\beta_c = 0.93$ instead of 0.95. After adjusting the calibrated parameters, the remaining parameters are estimated using the same data and method as in the benchmark case.[3] The results of these alternative calibrations show that changing the calibrated values in the model does not have any significant effect on the results highlighted in the paper.

We study the effects of changing the calibration of these parameters in four ways. First, we present information on the posterior distributions from each estimation, which can be seen in Table 1. Second, we compare the impulse responses calculated from these estimates with the benchmark case in Figures 7 to 9. Third, we present the underlying states of each calibration alternative in Figures 10 to 15. Finally, we conduct the same counterfactual as in Section 6 of the main paper to analyze the importance of stochastic volatility shocks in explaining the house price volatility during the Great Recession under each calibration alternative in Figures 16 to 18.

As the posterior estimates show in Table 1, the values are similar across alternative calibrations compared to the baseline case. Then we use these estimates from the alternative calibrations to calculate impulse response functions. The GIRFs from the alternative calibrations are plotted along with the baseline results in Figures 7 to 9. As the figures show, the impulse responses are qualitatively similar to those of the baseline case. One noticeable difference is that the collateral constraint uncertainty shock has a smaller magnitude impact when the discount rates for unconstrained households and entrepreneurs are lower, as can be seen in Figure 7. The smaller magnitude is likely due to the steady state level of loans being 25% lower

[3]Due to the computational burden, 100,000 draws are done following the burn-in period instead of 170,000 as is done in the main paper.

with the alternate calibration. In this alternative calibration with the lower discount factor for the unconstrained households, they become less patient, and therefore, save less. Given that lower available funding also decreases lending, tightening of credit conditions cannot affect the economy as much. Therefore, the effects of the collateral constraint uncertainty decline. Another difference we can observe between the alternative calibrations and the baseline model is when the discount rate for constrained households is lower, as in calibration 3. In this calibration, the magnitude of impact of the intertemporal preference shock is somewhat larger than the baseline case, however the results are qualitatively similar. Part of the difference can be attributed to the lower level of housing held by the even more impatient constrained household under this calibration. Since the constrained households cannot demand as much housing, entrepreneurs end up with more housing, and therefore, borrowing a bigger share of loans. Overall, the uncertainty results in a larger decline in investment due to increased housing holdings of entrepreneurs.

The comparison of the underlying states from the alternative calibrations to the baseline case in the main paper can be seen in Figures 10 to 15. The underlying states for each alternative calibration look very similar to the baseline results from the main paper. The only noticeable difference is with the collateral constraint shock, m, in Figure 10 which falls by more after 2010 in the first alternative calibration where we have more impatient unconstrained households and entrepreneurs. The larger decline is, not surprisingly, combined with an increase in stochastic volatility for the collateral constraint shock as can be seen in Figure 11. This difference is due to the steady state level of lending being lower, as mentioned above, which means that changes in the collateral constraint will have a smaller effect on borrowing and economic activity.

The final way to understand what role the calibrated parameters play in the estimation results is to perform the counterfactual study completed in Section 6 of the main paper. In these counterfactual exercises, our goal is to understand the role of stochastic volatility shocks in house price volatility observed during the Great Recession for each alternative calibration. As can be seen in Figures 16 to 18, the results are very similar to that of the baseline estimation from Figure 7 from the main paper. In each case, the removal of stochastic volatility shocks

greatly reduces the observed house price volatility during the 2007 to 2011 time period. In other words, stochastic volatility shocks explain a large portion of the house price volatility during the Great Recession, regardless of the calibration values used in the paper.

Table 1: Posterior Distribution: Alternative Calibrations

	Baseline	Alt. 1	Alt. 2	Alt. 3		Baseline	Alt. 1	Alt. 2	Alt. 3		Baseline	Alt. 1	Alt. 2	Alt. 3
$\bar{a}$	0.0017	0.0001	0.0002	0.0009	ρ_{ϱ}	0.950	0.952	0.950	0.938	ν_{ϱ}	0.447	0.549	0.539	0.547
	-0.0006	-0.0001	-0.0002	-0.0005		(0.006)	(0.003)	(0.012)	(0.005)		(0.041)	(0.004)	(0.010)	(0.006)
$\bar{x}$	0.0020	0.0034	0.0039	0.0030	ρ_m	0.414	0.393	0.365	0.399	ν_m	0.599	0.629	0.659	0.635
	-0.0011	-0.0001	-0.0001	-0.0003		(0.030)	(0.002)	(0.007)	(0.011)		(0.036)	(0.002)	(0.005)	(0.021)
ν	0.100	0.102	0.101	0.103	ρ_j	0.233	0.242	0.269	0.255	ν_j	0.373	0.392	0.389	0.388
	(0.002)	(0.001)	(0.000)	(0.002)		(0.008)	(0.003)	(0.006)	(0.007)		(0.040)	(0.002)	(0.002)	(0.002)
α	0.589	0.577	0.581	0.578	ρ_{φ}	0.916	0.941	0.950	0.942	ν_{φ}	0.470	0.425	0.419	0.437
	(0.006)	(0.000)	(0.002)	(0.001)		(0.009)	(0.001)	(0.006)	(0.003)		(0.030)	(0.001)	(0.007)	(0.002)
$\bar{j}$	0.081	0.077	0.089	0.080	σ_{ϱ}	0.020	0.022	0.019	0.020	ν_A	0.784	0.801	0.789	0.798
	(0.009)	(0.003)	(0.003)	(0.007)		(0.005)	(0.000)	(0.001)	(0.001)		(0.012)	(0.001)	(0.006)	(0.004)
ζ	0.144	0.141	0.153	0.120	σ_m	0.033	0.032	0.031	0.034	ν_X	0.127	0.147	0.157	0.165
	(0.010)	(0.003)	(0.004)	(0.005)		(0.001)	(0.000)	(0.001)	(0.001)		(0.025)	(0.003)	(0.004)	(0.013)
ϕ_h	0.096	0.087	0.088	0.087	σ_j	0.361	0.365	0.372	0.366	ν_{ω}	0.533	0.504	0.511	0.505
	(0.005)	(0.000)	(0.000)	(0.001)		(0.007)	(0.000)	(0.001)	(0.000)		(0.015)	(0.005)	(0.003)	(0.006)
ψ_k	4.403	4.397	4.373	4.399	σ_{φ}	0.025	0.023	0.026	0.024	η_{ϱ}	2.317	2.465	2.439	2.483
	(0.019)	(0.002)	(0.003)	(0.006)		(0.005)	(0.000)	(0.001)	(0.001)		(0.054)	(0.003)	(0.013)	(0.005)
θ	0.612	0.584	0.606	0.592	σ_A	0.040	0.040	0.039	0.040	η_m	1.414	1.427	1.416	1.424
	(0.013)	(0.007)	(0.005)	(0.006)		(0.002)	(0.000)	(0.001)	(0.001)		(0.014)	(0.005)	(0.007)	(0.009)
ψ_R	0.162	0.140	0.143	0.161	σ_X	0.046	0.055	0.054	0.052	η_j	2.157	2.260	2.274	2.271
	(0.033)	(0.001)	(0.012)	(0.006)		(0.003)	(0.001)	(0.001)	(0.001)		(0.062)	(0.006)	(0.010)	(0.005)
ψ_y	0.707	0.604	0.583	0.620	σ_{ω}	0.015	0.020	0.026	0.023	η_{φ}	1.203	1.264	1.251	1.239
	(0.041)	(0.005)	(0.006)	(0.007)		(0.004)	(0.001)	(0.000)	(0.001)		(0.040)	(0.005)	(0.004)	(0.012)
ψ_{π}	4.450	4.502	4.522	4.518	η_{ω}	0.759	0.732	0.717	0.732	η_A	0.615	0.629	0.611	0.610
	(0.019)	(0.004)	(0.007)	(0.008)		(0.019)	(0.001)	(0.004)	(0.003)		(0.014)	(0.005)	(0.007)	(0.009)
										η_X	0.926	1.153	1.158	1.147
											(0.013)	(0.004)	(0.005)	(0.007)

Note: The table displays the posterior mode with the standard deviation of the posterior distribution in parentheses beneath.

Figure 10: Underlying States for Alternative Calibration 1: Level Shocks

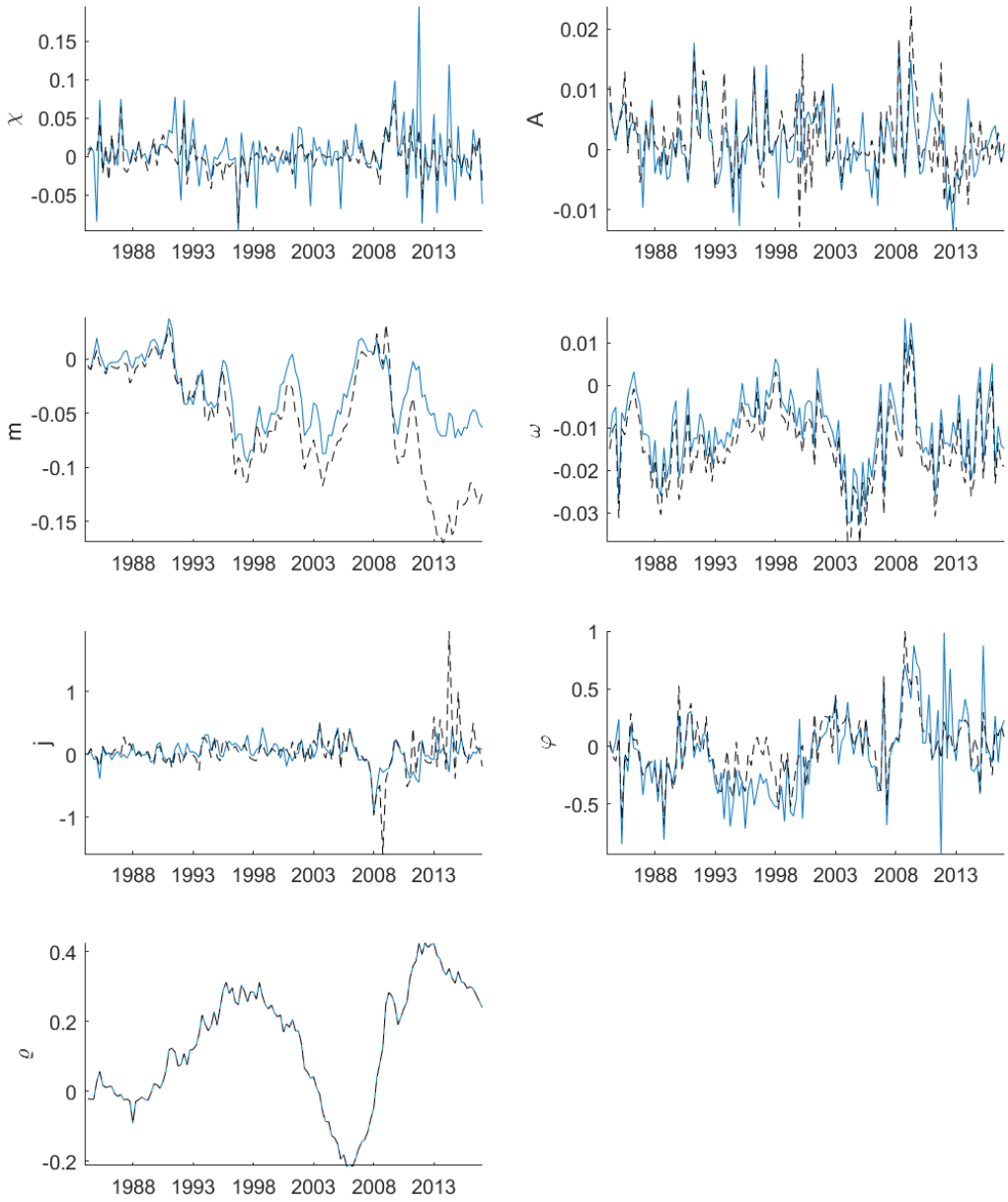

Note: Smoothed underlying states of the level shocks in log deviation from the mean form. They are calculated at the posterior mode. The median filtered states are shown. The black, dashed line is calculated using the estimation results from the first alternative calibration where $\beta = 0.985$ and $\gamma = 0.975$.

Figure 7: Responses of Macroeconomic Variables to Uncertainty Shocks: Alternative Calibration 1

(a) Housing Demand Uncertainty Shock (j)

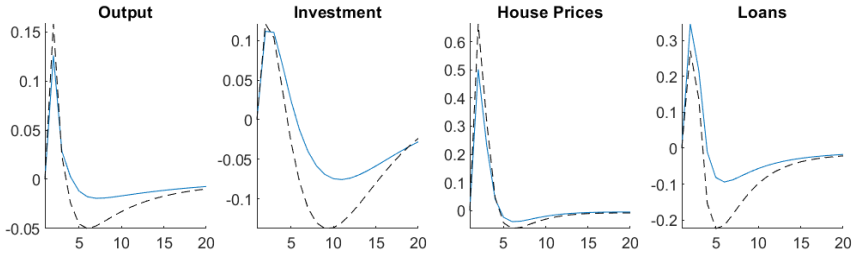

(b) Collateral Constraint Uncertainty Shock (m)

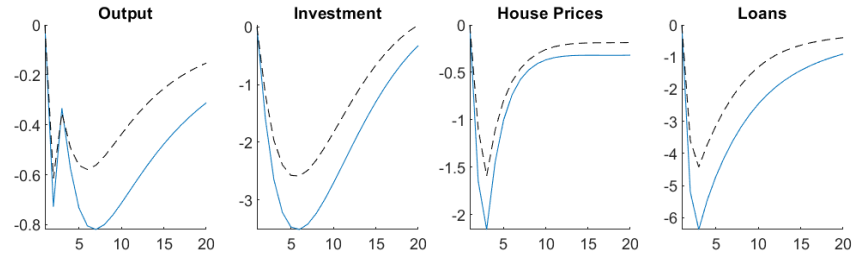

(c) Intertemporal Preference Uncertainty Shock (ϱ)

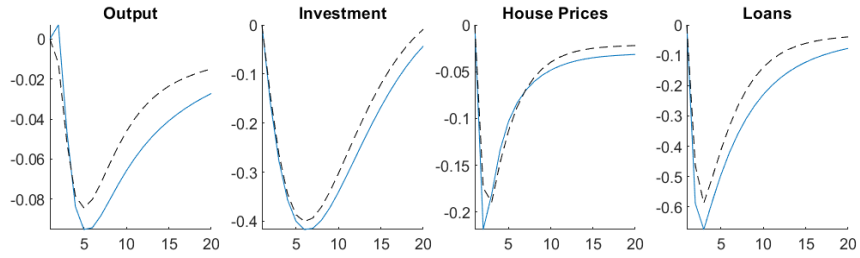

Note: The figure plots the generalized impulse responses of selected variables to a one standard deviation increase in innovation of correspondent shocks. The black, dashed line is calculated using the estimation results from the first alternative calibration where $\beta = 0.985$ and $\gamma = 0.975$. All coefficients are set to the posterior mode. The responses are calculated at the unconditional mean of the states. All responses are normalized so that the units of the vertical axis are percentage deviations from the steady-state.

Figure 8: Responses of Macroeconomic Variables to Uncertainty Shocks: Alternative Calibration 2

(a) Housing Demand Uncertainty Shock (j)

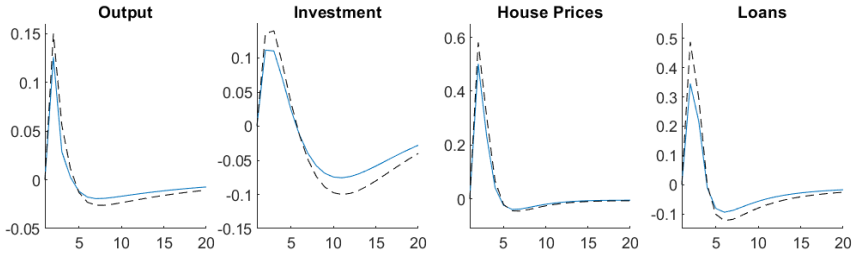

(b) Collateral Constraint Uncertainty Shock (m)

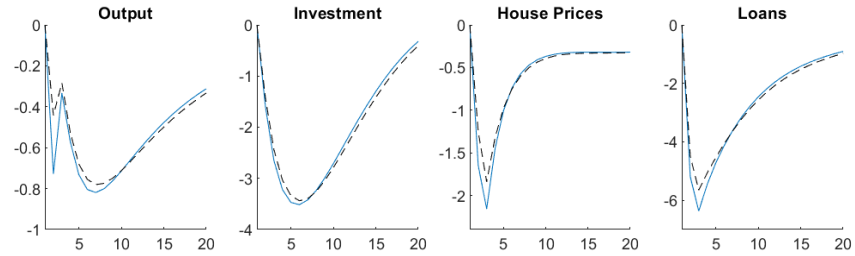

(c) Intertemporal Preference Uncertainty Shock (ϱ)

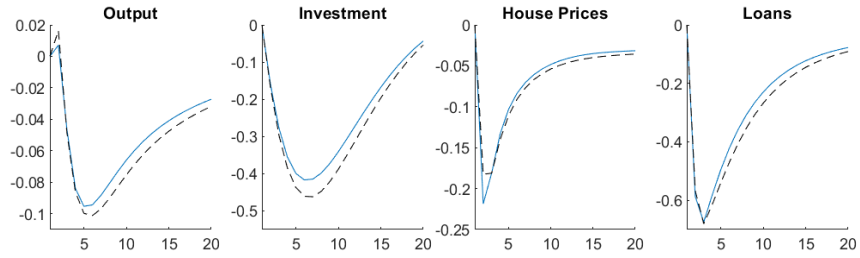

Note: The figure plots the generalized impulse responses of selected variables to a one standard deviation increase in innovation of correspondent shocks. The black, dashed line is calculated using the estimation results from the second alternative calibration where $\epsilon = 11$ and $\eta_c = \eta_u = 2$. All coefficients are set to the posterior mode. The responses are calculated at the unconditional mean of the states. All responses are normalized so that the units of the vertical axis are percentage deviations from the steady-state.

Figure 9: Responses of Macroeconomic Variables to Uncertainty Shocks: Alternative Calibration 3

(a) Housing Demand Uncertainty Shock (j)

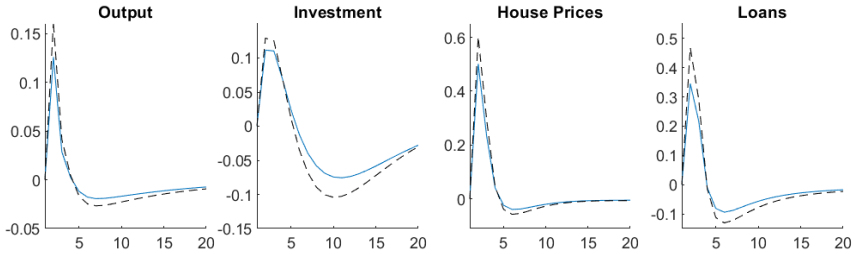

(b) Collateral Constraint Uncertainty Shock (m)

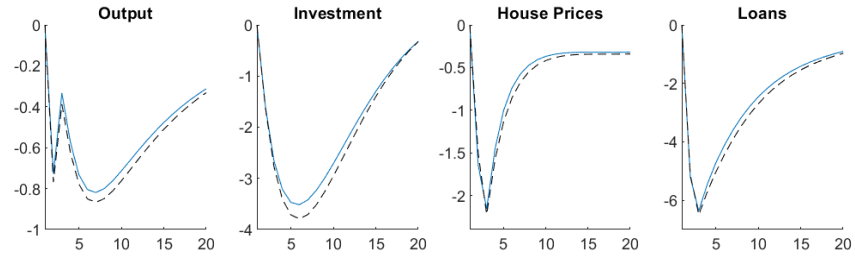

(c) Intertemporal Preference Uncertainty Shock (ϱ)

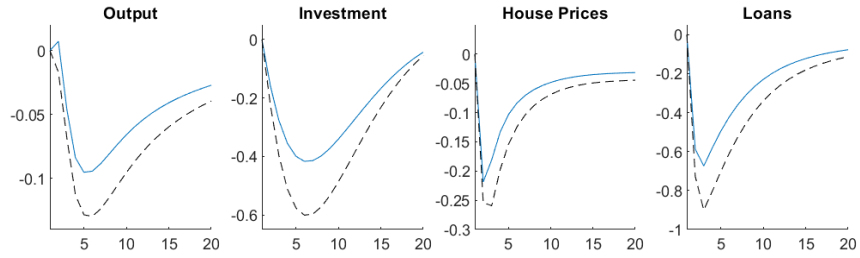

Note: The figure plots the generalized impulse responses of selected variables to a one standard deviation increase in innovation of correspondent shocks. The black, dashed line is calculated using the estimation results from the third alternative calibration where $\beta_c = 0.93$. All coefficients are set to the posterior mode. The responses are calculated at the unconditional mean of the states. All responses are normalized so that the units of the vertical axis are percentage deviations from the steady-state.

Figure 11: Underlying States for Alternative Calibration 1: Stochastic Volatility

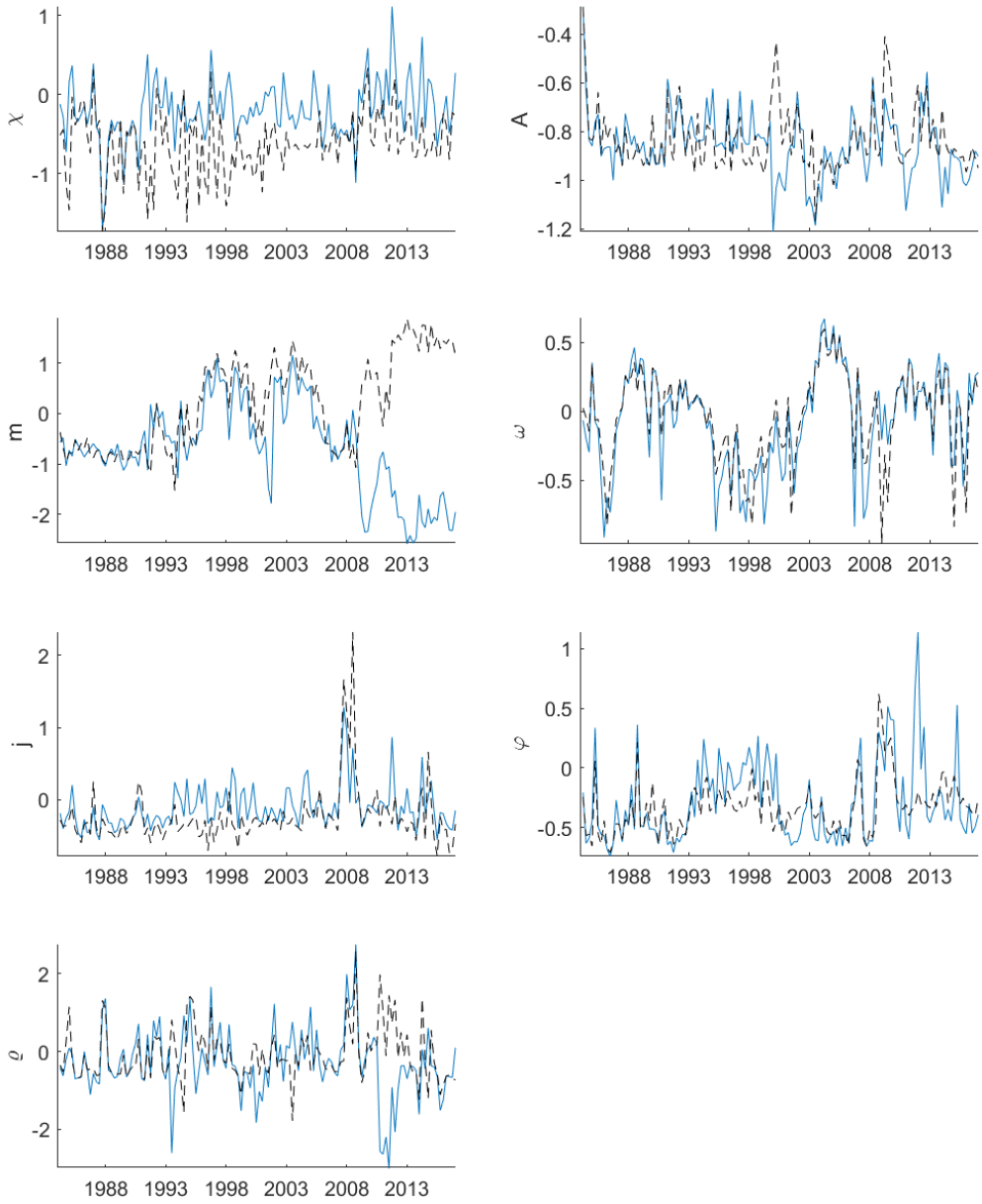

Note: Smoothed underlying states of the stochastic volatility shocks in log deviation from the mean form. They are calculated at the posterior mode. The median filtered states are shown. The black, dashed line is calculated using the estimation results from the first alternative calibration where $\beta = 0.985$ and $\gamma = 0.975$.

Figure 12: Underlying States for Alternative Calibration 2: Level Shocks

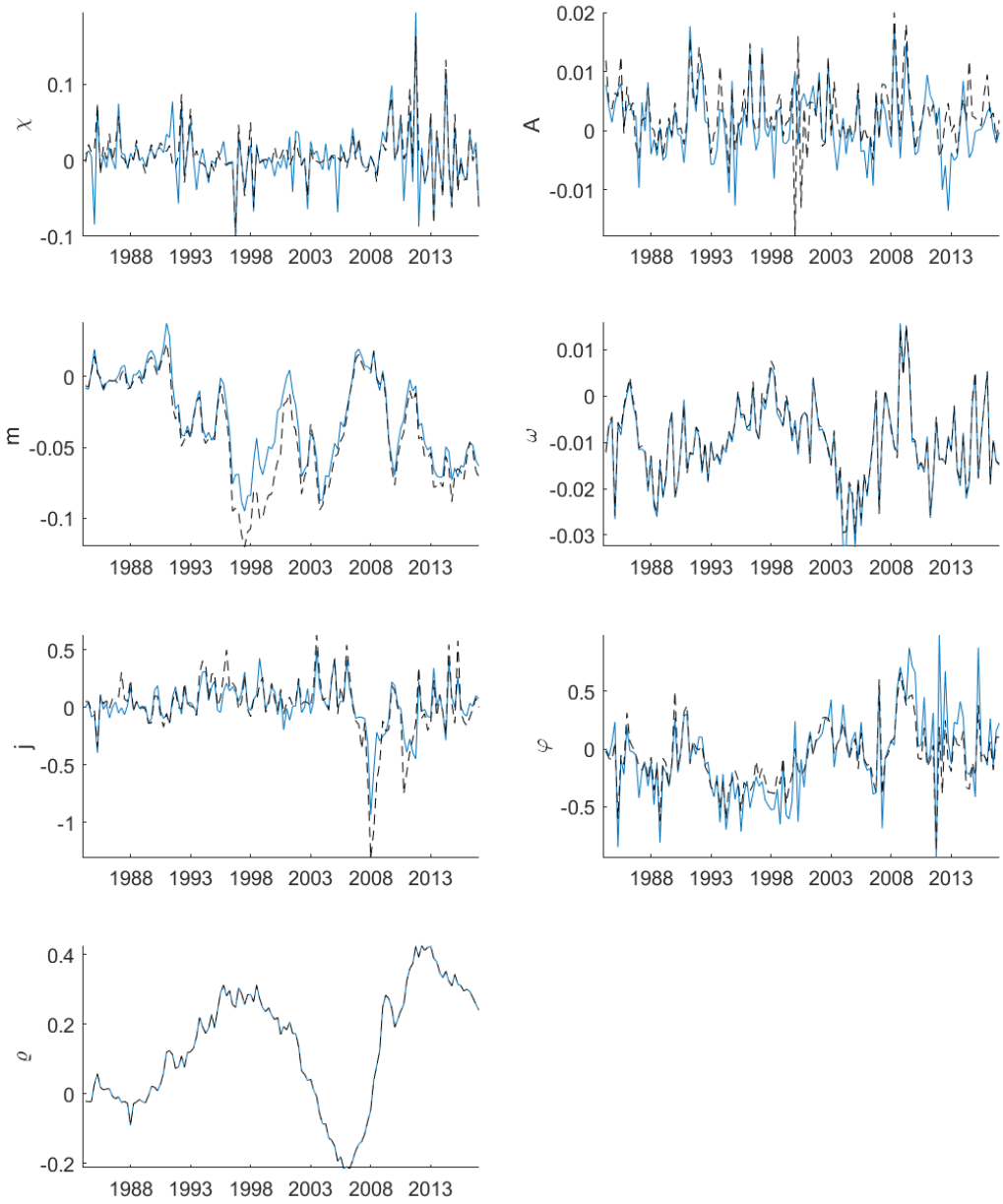

Note: Smoothed underlying states of the level shocks in log deviation from the mean form. They are calculated at the posterior mode. The median filtered states are shown. The black, dashed line is calculated using the estimation results from the second alternative calibration where $\epsilon = 11$ and $\eta_c = \eta_u = 2$.

Figure 13: Underlying States for Alternative Calibration 2: Stochastic Volatility

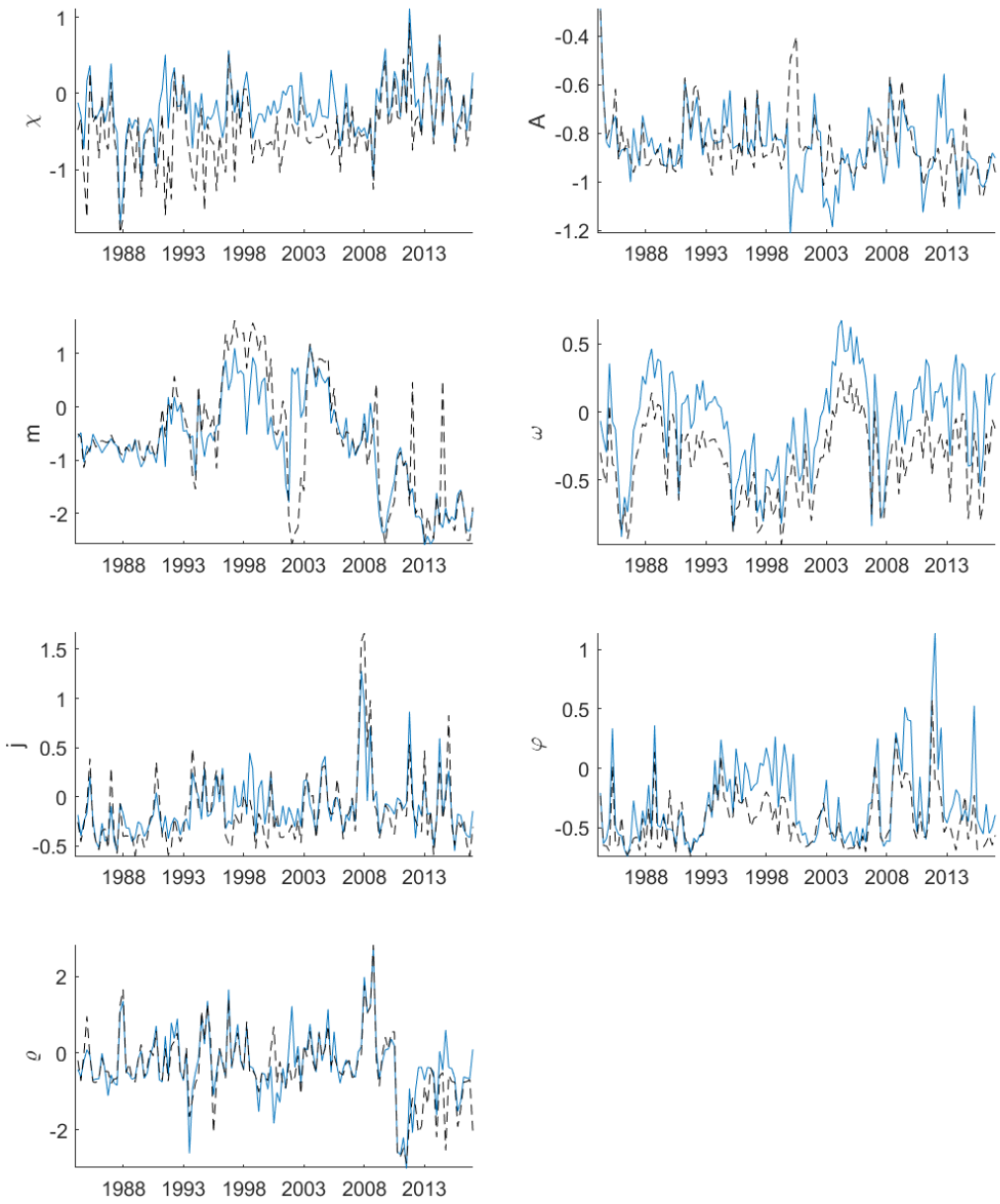

Note: Smoothed underlying states of the stochastic volatility shocks in log deviation from the mean form. They are calculated at the posterior mode. The median filtered states are shown. The black, dashed line is calculated using the estimation results from the second alternative calibration where $\epsilon = 11$ and $\eta_c = \eta_u = 2$.

Figure 14: Underlying States for Alternative Calibration 3: Level Shocks

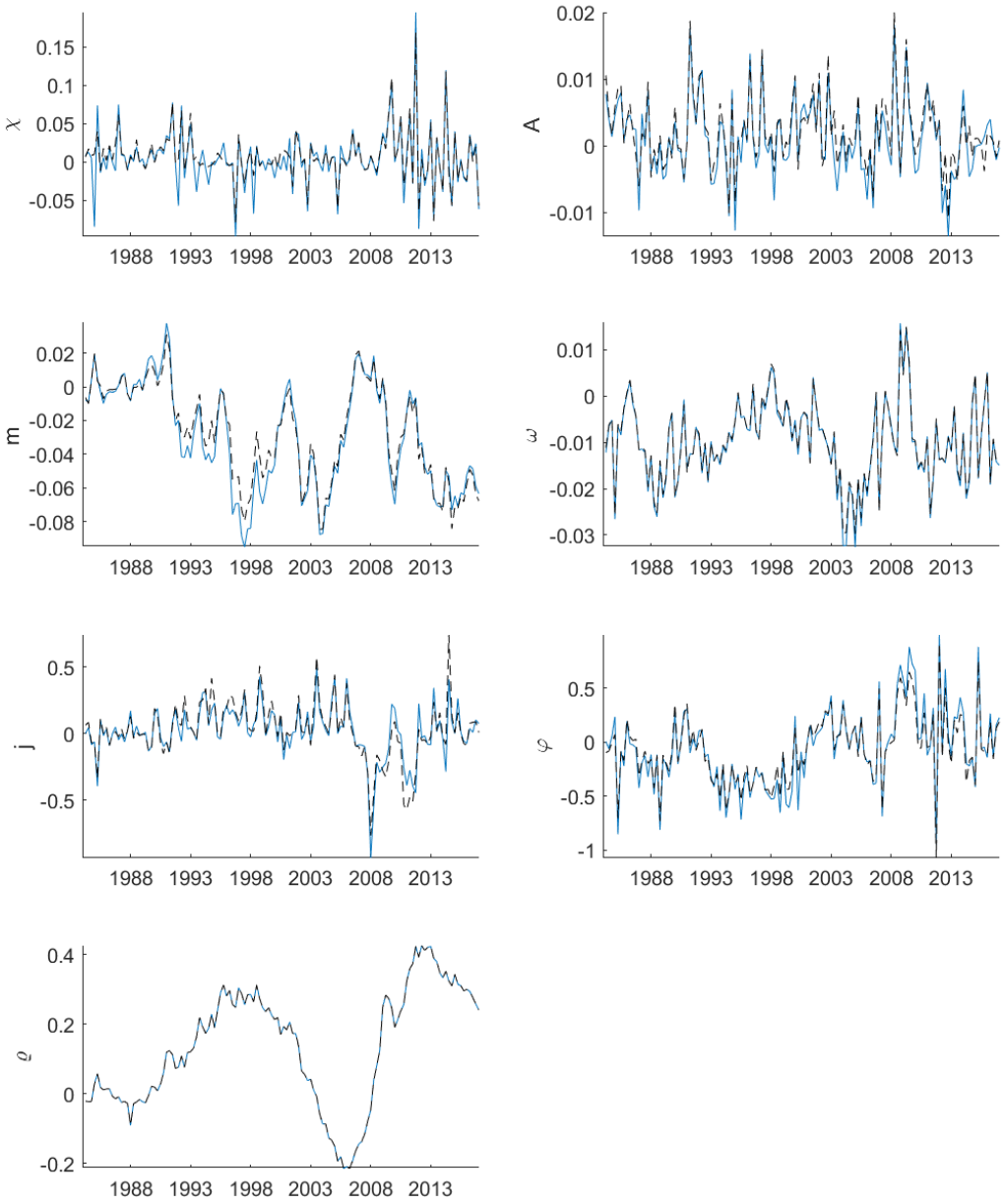

Note: Smoothed underlying states of the level shocks in log deviation from the mean form. They are calculated at the posterior mode. The median filtered states are shown. The black, dashed line is calculated using the estimation results from the third alternative calibration where $\beta_c = 0.93$.

Figure 15: Underlying States for Alternative Calibration 3: Stochastic Volatility

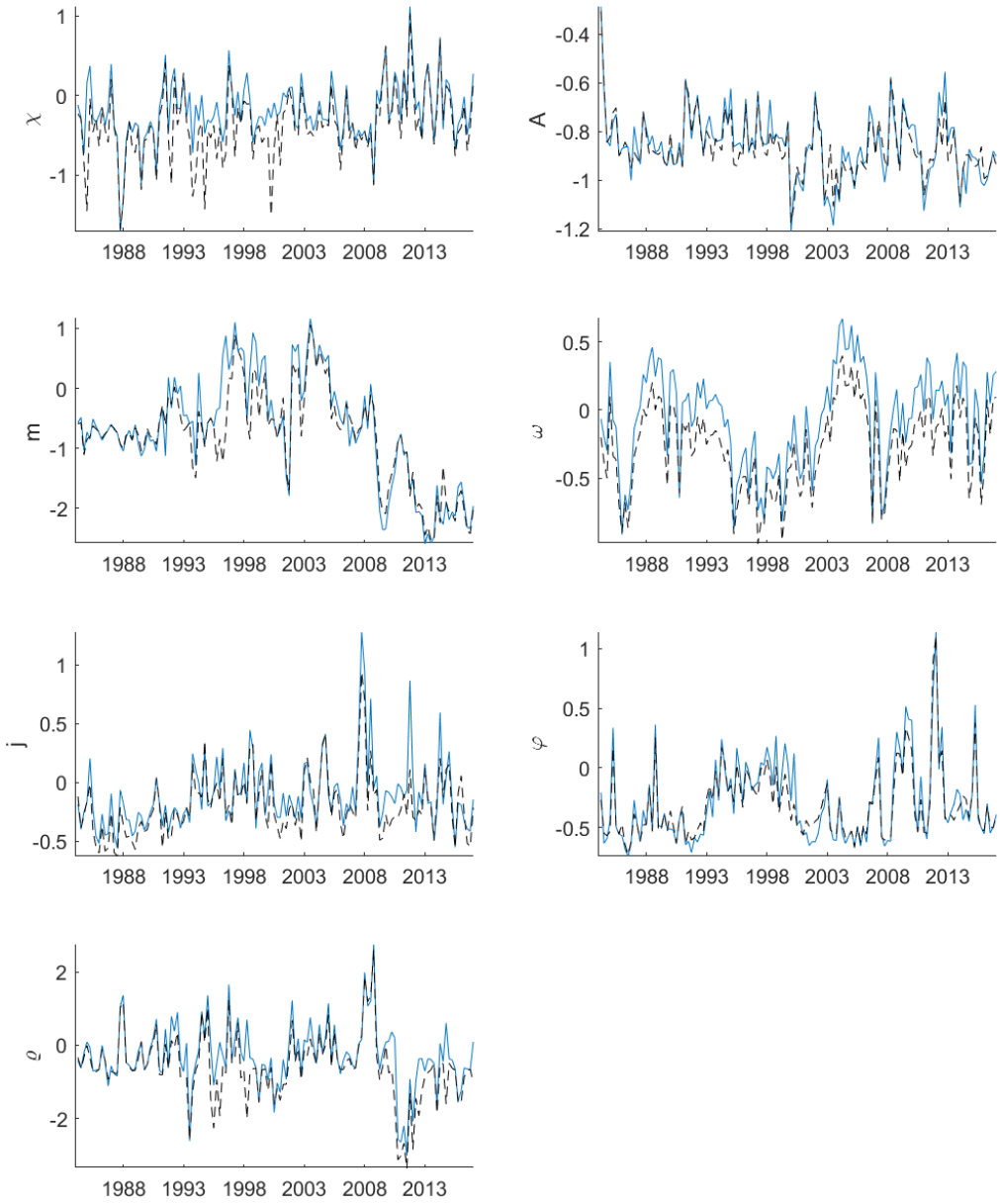

Note: Smoothed underlying states of the stochastic volatility shocks in log deviation from the mean form. They are calculated at the posterior mode. The median filtered states are shown. The black, dashed line is calculated using the estimation results from the third alternative calibration where $\beta_c = 0.93$.

Figure 16: Counterfactual Study: Alternative calibration 1

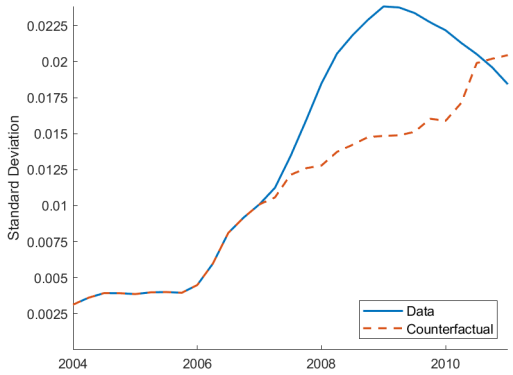

Note: Rolling 6-year standard deviation of house price growth. The blue, solid line represents the actual data. The red, dashed line is generated from the simulated model using the underlying filtered shocks, except the stochastic volatility shocks, which are set to zero from 2007Q1 to 2010Q4. The estimation results from the first alternative calibration where $\beta = 0.985$ and $\gamma = 0.975$ are used to calculate the filtered shocks.

Figure 17: Counterfactual Study: Alternative calibration 2

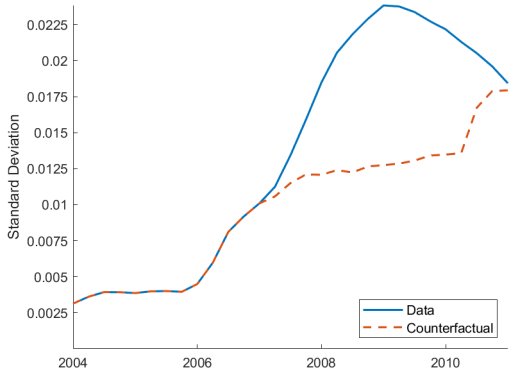

Note: Rolling 6-year standard deviation of house price growth. The blue, solid line represents the actual data. The red, dashed line is generated from the simulated model using the underlying filtered shocks, except the stochastic volatility shocks, which are set to zero from 2007Q1 to 2010Q4. The estimation results from the second alternative calibration where $\epsilon = 11$ and $\eta_c = \eta_u = 2$ are used to calculate the filtered shocks.

Figure 18: Counterfactual Study: Alternative calibration 3

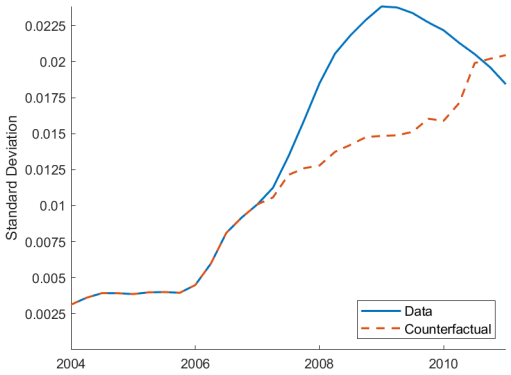

Note: Rolling 6-year standard deviation of house price growth. The blue, solid line represents the actual data. The red, dashed line is generated from the simulated model using the underlying filtered shocks, except the stochastic volatility shocks, which are set to zero from 2007Q1 to 2010Q4. The estimation results from the third alternative calibration where $\beta_c = 0.93$ is used to calculate the filtered shocks.

References

Fernández-Villaverde, Jesús, and Juan F. Rubio-Ramírez (2007) 'Estimating Macroeconomic Models: A Likelihood Approach.' *The Review of Economic Studies* 74(4), 1059–1087

Fernández-Villaverde, Jesús, Pablo Guerrón-Quintana, and Juan F Rubio-Ramírez (2015) 'Estimating dynamic equilibrium models with stochastic volatility.' *Journal of Econometrics* 185(1), 216–229

Gust, Christopher, Edward Herbst, David Lpez-Salido, and Matthew E. Smith (2017) 'The empirical implications of the interest-rate lower bound.' *American Economic Review* 107(7), 1971–2006

Plante, Michael, Alexander W. Richter, and Nathaniel A. Throckmorton (2017) 'The Zero Lower Bound and Endogenous Uncertainty.' *The Economic Journal* 128(611), 1730–1757